

# The Importance of Fabricating Hard Carbon-Based Full Cells to Overcome Sodium Metal Anode Limitations in Evaluating High-Mass-Loading Cathodes

Huiya Yang, Yuejing Zeng, Wei Li, Yang Yang,\* and Jinbao Zhao\*



Cite This: *ACS Energy Lett.* 2025, 10, 2868–2876



Read Online

ACCESS |



Metrics & More

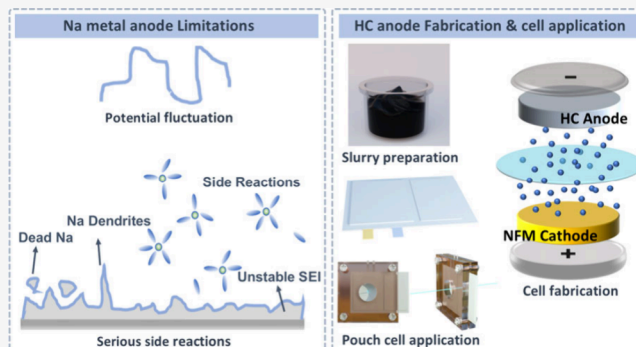


Article Recommendations



Supporting Information

**ABSTRACT:** Developing advanced cathode materials is pivotal for successful commercialization of sodium-ion batteries (SIBs), but it requires reliable evaluation of electrochemical performance. However, the widely used sodium metal anode in academic research is not a “qualified counter electrode”, particularly under high-mass-loading and limited-Na conditions. Herein, the limitations of Na metal anode are discussed, and reliable high-mass-loading hard carbon (HC)-based full cells are proposed with a detailed guideline provided for qualified slurry preparation, electrode fabrication, and cell design. Three-electrode tests reveal Na metal’s severe potential fluctuations, which influences the evaluation of electrochemical performance for high-mass-loading  $\text{NaNi}_{1/3}\text{Fe}_{1/3}\text{Mn}_{1/3}\text{O}_2$  cathodes. Encouragingly, HC-based pouch cells demonstrate good electrochemical performance, including lower polarization ( $\sim 0.07 \Omega$  ohmic resistance), enhanced cycling stability (85% retention after 250 cycles), and rate performance (80% capacity maintained at 4 C), highlighting the exceptional reliability and suitability. This study offers a robust methodology for evaluating lab-developed cathode materials, bridging the gap between academia and industrial applications.



Large-scale electrochemical energy storage systems play a crucial role in regulating peak load transfer in renewable energy generation, which is often characterized by intermittent output.<sup>1,2</sup> Unlike portable electronic devices and electric vehicles dominated by lithium-ion batteries (LIBs), large-scale energy storage prioritizes the operating cost and cycling life over energy density. In this context, sodium-ion batteries (SIBs) have emerged as a promising alternative to LIBs due to their comparable electrochemical properties and cost-effectiveness of sodium resources.<sup>3</sup> Specifically, the development of advanced cathode materials and their modification strategies has garnered considerable attention, as these materials directly determine both the energy density and operating cost of SIBs.<sup>2,4–9</sup>

In the academic community, the most commonly used method for evaluating cathode materials involves assembling sodium metal batteries, where Na metal serves as the counter electrode. However, the observed electrochemical performance of the cathode in this system is influenced by the entire cell and cannot exclude the effects of the Na metal anode.<sup>10–12</sup> For instance, in galvanostatic cycling tests, the monitored cell

voltage ( $E_{\text{cell}}$ ) is used to evaluate performance, but the actual cathode potential ( $E_{\text{cathode}}$ ) also depends on the plating and stripping potentials of the anode ( $E_{\text{cathode}} = E_{\text{cell}} - E_{\text{anode}}$ ). While the cell cutoff voltage remains constant, the voltage polarization at the sodium metal anode directly impacts the cathode charge cutoff potential, resulting in deviations in desodiation degrees and overall cycling performance. From an electrochemical prospect, the Na metal anode is not a “qualified counter electrode” due to the severe interface side reactions and potential fluctuations<sup>13–15</sup> (confirmed by the three-electrode-cell results using  $\text{NaTi}_2(\text{PO}_4)_3$  (NTP) as the reference electrode in this work). From the perspective of cost and energy density (Tables S1 and S2), developed

Received: February 13, 2025

Revised: May 13, 2025

Accepted: May 15, 2025

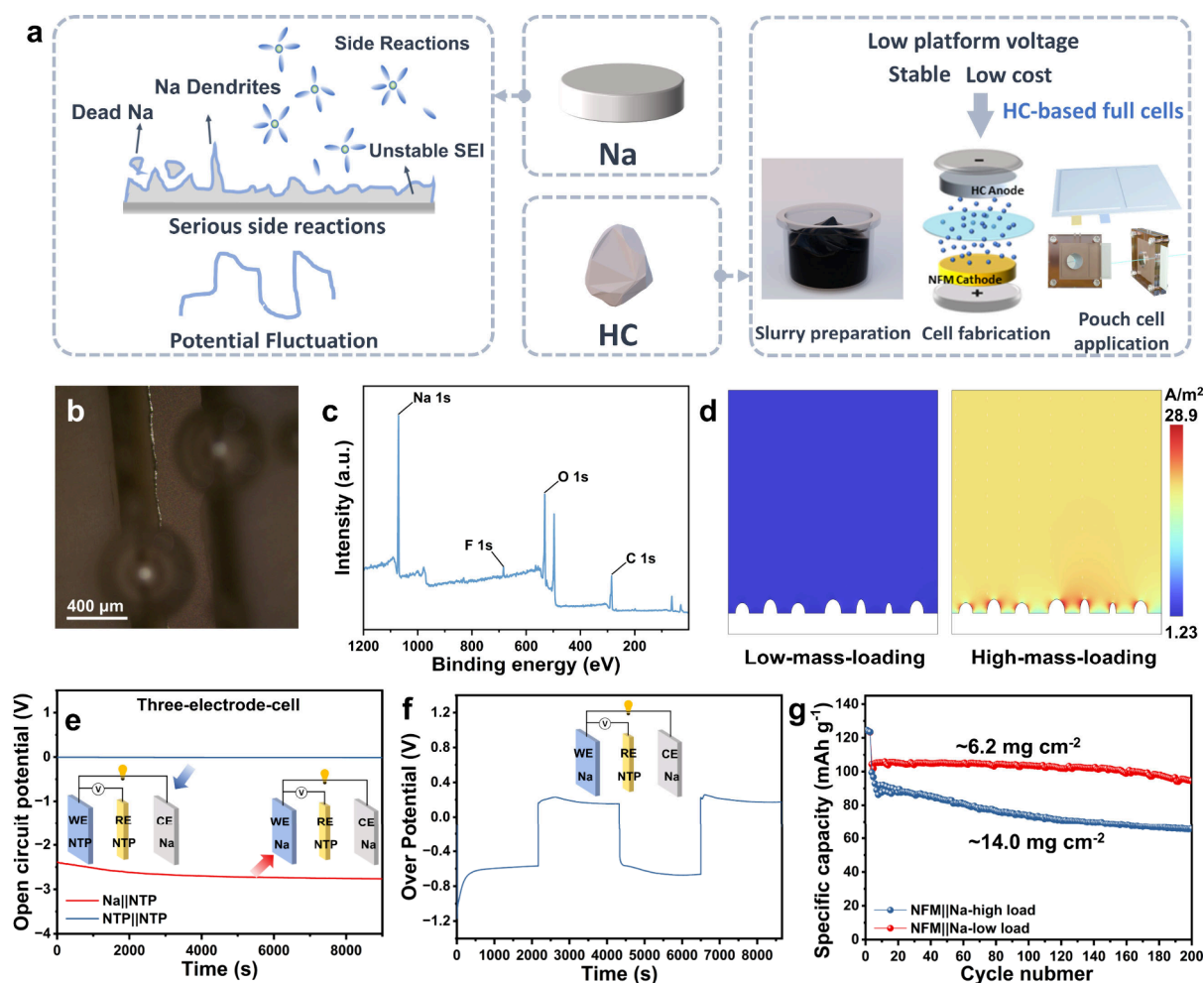


**Figure 1.** Impact of anode material and electrode mass loading on cell performance. (a) Comparison of Na metal and HC material. (b) In-situ optical microscopy image of bubble generation on Na metal immersed in electrolyte. (c) XPS result of Na metal after immersing in electrolyte. (d) Current density distributions in Na metal/electrolyte interphase with different area-capacity cathodes. (e) Open circuit potential of Na||NTP and NTP||NTP in a three-electrode cell. (f) Overpotential on Na electrode during the process of deposition and stripping. (g) Cycling performance of NFM cathode with different mass loadings.

cathode materials should be fabricated into high-mass-loading electrodes and pouch cells for practical applications rather than the low-mass-loading electrodes typically employed in laboratory evaluations. When coupled with such a high-mass-loading cathode, the plating capacity and current density on the Na metal anode significantly increase under the same C-rate, exacerbating Na dendrite growth and irreversible side reactions. Our preliminary tests, in which we assembled Na metal anodes with both high and low mass loadings of the same  $\text{NaNi}_{1/3}\text{Fe}_{1/3}\text{Mn}_{1/3}\text{O}_2$  (NFM) cathode material, reveal a pronounced discrepancy in cycling stability and voltage polarizations (Figure S1).

Hard carbon (HC)-based full batteries could be a more reliable platform for assessing cathode materials, particularly under high-mass-loading conditions. The HC anode offers a considerable  $\text{Na}^+$  storage capacity ( $\sim 300 \text{ mAh g}^{-1}$ ) with a relatively low platform voltage (0.1 V vs  $\text{Na}/\text{Na}^+$ ).<sup>16,17</sup> Furthermore, HC is composed of a highly disordered and distorted pseudographite structure (Figure S2a-c) with substantial interlayer spacing (Figure S2d), enabling it to accommodate sodium ions more effectively.<sup>18</sup> Thus, its limited volume expansion and low reactivity ensure high reversibility, allowing for an accurate assessment of the actual electro-

chemical performance of cathodes.<sup>19</sup> Therefore, establishing a comprehensive understanding of the principles governing HC-based full batteries in laboratory settings is critical and will undoubtedly drive the development of high-performance cathode materials. However, these aspects remain insufficiently explored to date.

In this work, the limitations of Na metal anodes are discussed, and the critical parameters for preparing high-mass-loading HC-based full cells in the laboratory are systematically investigated, including slurry preparation, electrode fabrication, and cell design (Figure 1a). As anticipated, metallic Na-based coin cells exhibit higher resistance and poor electrochemical performance compared to HC-based battery configurations. Moreover, HC-based pouch cells demonstrate superior cycling stability under high-loading-mass conditions compared to HC-based coin cells, indicating the excellent reliability of HC-based pouch cell configuration. Besides, in situ projective XRD measurements can be readily conducted on HC-based pouch cells, facilitating the study of electrochemical mechanisms. This study offers a robust methodology for evaluating lab-developed cathode materials and bridges the gap between scientific research and industrial applications.

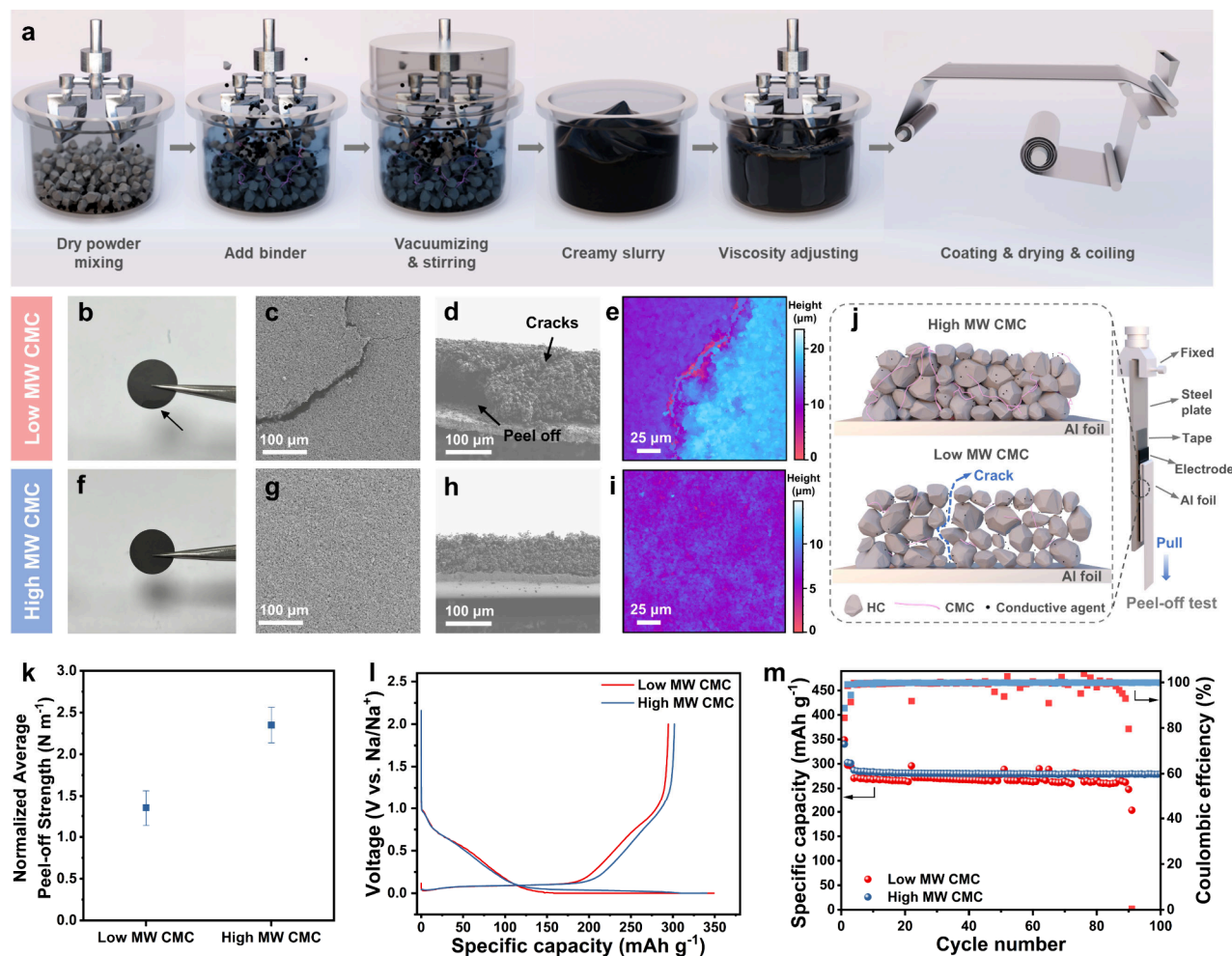
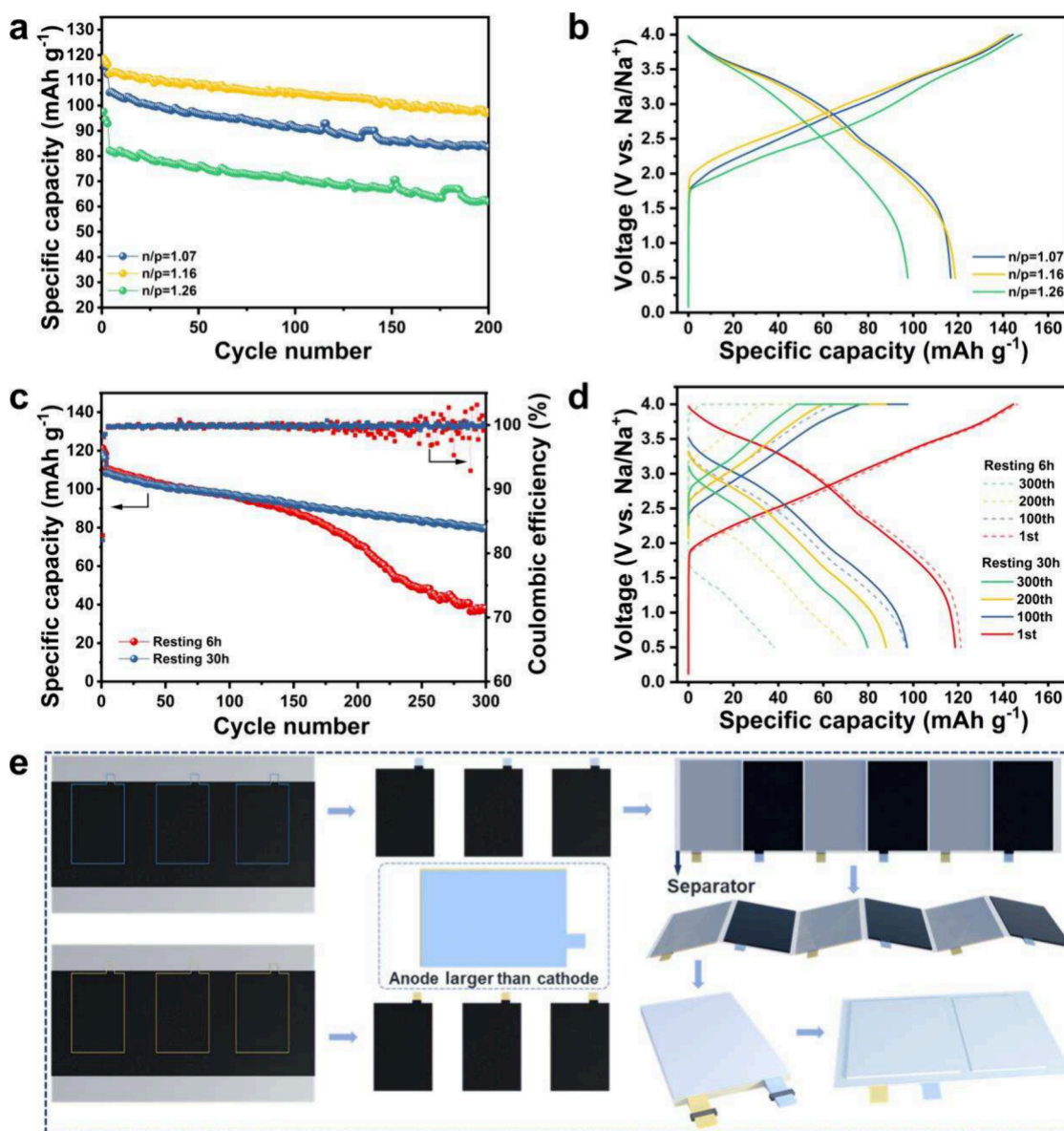


Figure 2. Impact of the fabrication procedure of slurry and electrode on cell performance. (a) Schematic diagram of the fabrication procedure of the slurry and electrode. Effect of binder MW on electrode: (b) digital photographs, (c) surface scanning electron microscopy (SEM) images, (d) cross-section images, and (e) laser scanning confocal microscopy (LSCM) surface topography images of HC electrode with low MW CMC binder, (f) Digital photographs, (g) surface SEM images, (h) cross-section images, and (i) LSCM surface topography images of HC electrode with high MW CMC binder; (j) Schematic diagram and (k) results of electrode peel-off strength test; (l) First-cycle charging and discharging curves and (m) cycling performance of HC with different MW CMC.

**The Limitations of Na Metal Anode.** The utilization of Na metal as an anode presents numerous challenges, including severe side reactions between Na metal and the electrolyte, dendritic Na formation, and the generation of “dead Na” during cycling. In-situ optical microscopy and X-ray photoelectron spectroscopy (XPS) are used to verify the serious side reactions between Na metal and electrolyte. As shown in Figures 1b,c and S3, noticeable bubbles and solid electrolyte interface (SEI) form on the surface of Na metal after immersing in the electrolyte. Under the real state of the high-area-capacity electrode, the issue becomes more pronounced. These issues are further exacerbated under high-area-capacity electrode conditions. The plating capacity and current density of the Na metal anode can be substantially enhanced by increasing the mass loading of the cathode material. The increased current density exacerbates the nonuniform distribution of ions and promotes dendrite growth (Figure 1d), thereby intensifying the by-reaction with electrolyte and the formation of “dead Na”.<sup>20</sup> When compared to the stable  $\text{NaTi}_2(\text{PO}_4)_3$  reference electrode (RE), the use of Na metal as a counter-electrode (CE) exhibits instability in open circuit potential (Figure 1e), resulting in significant fluctuations in

overpotential observed during the process of deposition and stripping particularly at the high current density (Figure 1f, Figure S4). In addition, as the electrode thickness increased, the internal resistance and the inhomogeneity of state of charge (SOC) distribution rose.<sup>21</sup> Ultimately, the specific capacity and cycling performance of Na metal cells vary with different mass-loading electrodes (Figure 1g).

Consequently, when coupled with high-mass-loading NFM cathodes, NFM||Na half cells demonstrate poor electrochemical performance (Figure S5), which is attributed to the high reactivity of Na metal, limited reversibility of its plating/stripping processes, and continuous consumption of the electrolyte. Furthermore, Na metal provides a large amount of  $\text{Na}^+$  and the cell is a nonstoichiometric sodium system, which introduces a bias in the assessment of the cathode materials. Therefore, Na metal is not the optimal anode choice for assessing the properties of cathode materials under real high-area-capacity conditions. Benefiting from the good structural stability of HC and high  $\text{Na}^+$ -insertion/extraction reversibility (as confirmed by the stable and small charge-transfer resistance ( $R_{ct}$ ), Figure S6), the NFM||HC exhibits excellent cyclic stability, rate performance, and lower voltage



**Figure 3.** Effect of factors on full cell performance. (a) Cycling performance and (b) first charge–discharge curves of a full coin cell with different N/P ratios. (c) Cycling performance and (d) charge–discharge curves of a full coin cell with different resting times. (e) Schematic diagram of pouch cell assembly.

polarizations. On these grounds, the significance of employing a high-area-capacity HC-based anode in lieu of a Na metal anode for assessing the electrochemical performance of cathode materials is elucidated.

**Qualified Slurry and Electrode Preparation.** Under high-loading conditions, additional factors, including electrode fabrication, formation of an effective conductive network, and ionic diffusion kinetics, also play critical roles in influencing cathode performance. Therefore, the preparation of slurry is the key technological issue in electrode manufacture, further impacting battery performance. A typical slurry consists of active materials, conductive agents, binders, and solvents that should be uniformly dispersed as a suspension. However, the difficulty escalates when preparing a homogeneous high-solid-content slurry to obtain a high mass-loading electrode, primarily due to the challenges encountered during the mixing process such as inadequate binder dissolution, particle agglomeration, and so on. And the poor slurry will result in

uneven electrode films, resulting in powder loss, cracking, and difficulty in forming an effective conductive network. Given that, a reliable homogenizing process of the slurry, which is seldom discussed in existing literature, is proposed with reference to industrial processes. And the key points in preparation are summarized as follows (Figures 2a and S7; Tables S3 and S4):

- (1) Dry powder mixing. The active materials and conductive agents are totally added and preliminarily mixed in the stirring tank.
- (2) Adding binder. The binder should be predissolved in a solvent and possess a relatively high initial viscosity.
- (3) Vacuumizing and stirring. The vacuum environment promotes liquid wetting of the solid powder surface and defoaming, thus promoting dispersion.
- (4) Viscosity adjusting. Appropriate amount of solvent is added to adjust the slurry viscosity to approximately 3000 cps.<sup>22</sup>

After the vacuumizing and stirring steps, the powder and binder are evenly mixed to form a creamy slurry (Figure S7), which is the key feature for a successful slurry. The shear stress during stirring could facilitate the uniform dispersion of active material and conductive agent, thus contributing to establishing an effective conductive network in electrode. Before the mixing process, the binder should be fully dissolved to prevent the viscosity of the binder from changing during slurry preparation. Attentionally, the viscosity of the slurry should be adjusted to an appropriate value, since excessively low viscosity will lead to insufficient loading and high porosity, while overly high viscosity may result in coating difficulties and defects due to poor flow dynamics. For most of the cathode materials that use polyvinylidene difluoride (PVDF) as binder, high air humidity should be avoided to prevent gelation of the slurry during the mixing process. Meanwhile, for anode materials, if carboxymethyl cellulose (CMC) and polymerized styrene butadiene rubber (SBR) are employed as binders, it is advisable to refrain from prolonged high-speed stirring, as this will lead to the structural damage of SBR. Once the qualified slurry is prepared, coating and drying should promptly proceed to achieve a high mass-loading electrode.

In addition to the acquisition of slurry, a lot of details also affect the successful preparation of a qualified electrode.<sup>10,23,24</sup> For instance, the molecular weight (MW) of the binder will significantly affect the robustness of the electrodes. In particular, there is a reduced binder content in the high mass-loading electrodes, thus amplifying the influence that adhesive strength of binder has on the viscosity of the slurry and the adhesion of the electrodes. In order to simplify the discussion, commercial HC materials with superior electrochemical performance (Figure S8) are used to prepare electrode with two CMC binders. As presented in Figure 2b-i, the MW of the CMC binder exerts a significant impact on the morphology of the HC electrode. After the drying process, numerous cracks appear on the surface of the high-mass-loading HC electrode prepared using low-MW CMC (Figures 2b-d, S9), whereas that with high-MW CMC binder maintains a smooth surface (Figure 2f-h). Furthermore, laser scanning confocal microscopy (LSCM) is employed to map the roughness of the electrode surface (Figure 2e and i). As shown in Figure 2e, the electrode prepared using low-MW CMC exhibits severe deviation in height, which can be attributed to the inadequate adhesive strength of low-MW CMC. By contrast, there is no significant fluctuation on the surface of the HC electrode with high-MW CMC binder (Figure 2i). In addition, the adhesion between the active materials and the current collectors is evaluated by 180° peel-off tests (Figure 2j). As illustrated in Figure 2k, the normalized average peel-off strength of the electrode prepared by low-MW CMC ( $1.35 \text{ N cm}^{-1}$ ) is obviously smaller than that of high-MW CMC ( $2.35 \text{ N cm}^{-1}$ ), indicating the relationship between the adhesive strength and MW of the binder. The presence of cracks will disrupt the continuity of conductive network within the electrode, while the loose structure may further accelerate the active material loss and capacity fading. As a result, the high mass-loading HC electrode with a low-MW CMC binder and poor mechanical strength exhibits a worse cycle performance in half cells, and the capacity diminishes to zero rapidly after 90 cycles, with repeated appearance of “soft short circuit” during cycling due to the nonuniform conductive network (Figures 2l,m and S10). The high-MW CMC, which has a higher adhesive strength and viscosity, is more suitable for the

preparation of high-mass-loading HC electrodes. But it should be noted that the overhigh MW of binder will result in excessive viscosity and poor fluidity of slurry with the same solid content,<sup>25</sup> which leads to the uneven stripes on electrode. Considering the properties of active materials and conductive agents, it is necessary to carefully select a suitable type and MW of binder.<sup>26</sup>

**Design and Assembly of Full Cells.** The assembly of the full cell is similar to that of the coin half cell. In order to optimize the utilization of the cathode material, the anode area is typically larger than the cathode. From the perspective of battery safety, the capacity of the negative electrode is usually designed higher than that of the positive electrode. However, an overly high N/P ratio can lead to a significant reduction in the energy density of the battery. Besides, the relatively low first-cycle Coulombic efficiency of the HC anode will lead to an increase in irreversible capacity loss when the N/P ratio is higher.<sup>27</sup> Therefore, the areal-capacity ratio of negative and positive electrodes (N/P ratio) is a critical factor for the capacity of full cell.<sup>28,29</sup> Based on the actual specific capacity (Figure S11) and the areal mass loading of cathode (NFM) and anode (HC), full cells with different N/P ratios are designed, as shown in Figure 3a,b. Optimal specific capacity and cycling performance can be achieved when the N/P is approximately 1.16. However, when N/P = 1.26, the full cell delivers a large irreversible capacity loss (the specific capacity is only  $82 \text{ mAh g}^{-1}$  at 1 C) due to an excess of anode. In addition, the cycling performance will be affected by the resting time (interval between the cell assembly and the commencement of electrochemical testing). In the first two activated cycles (0.1 C), the full cell of resting 6 h delivers similar capacity to that of resting 30 h (Figure 3c,d); however, the cell of resting 6 h degrades rapidly after 150 cycles (only 34% cycle retention after 300 cycles). The high-mass-loading electrode exhibits a slower electrolyte wetting rate compared to the low-mass-loading electrode due to its overall thickness. After 6 h of resting, the majority of the electrode surface becomes saturated but is insufficient for achieving uniform wetting within the electrode. The inhomogeneity of wetting has a minimal influence on cell capacity for the first charging–discharging cycle due to the minimal applied current density. Nevertheless, as a large current is applied for the long-term cycling periods, the ion diffusion rate in the electrolyte surpasses that in the bulk phase of the electrode, resulting in a significant impact arising from the inhomogeneity of the wetting situation.

Considering the practical application, evaluation results in pouch cells are more realistic than those in coin cells. Besides, the larger resistance of the coin cell also leads to a non-negligible deviation from real cycling stability and rate performance. The NFM|HC laminated full pouch cells with a N/P ratio of 1.16 are assembled as following steps (Figure S12): First, the prepared electrodes are punched as suitable pieces by regular dies (Figure 3e), and a small part of the collector is reserved for welding later. Generally, the area of negative electrode is slightly larger than that of positive electrode to ensure the utilization of cathode material. Second, a piece of separator is cut, whose width is slightly larger than cathode and anode, and length is longer than the combined width of electrodes. Next, a piece of anode is placed on one side of the separator, followed by folding the separator discretely to cover the anode. Then the cathode is stacked on top of the separator, and the separator is folded again to cover

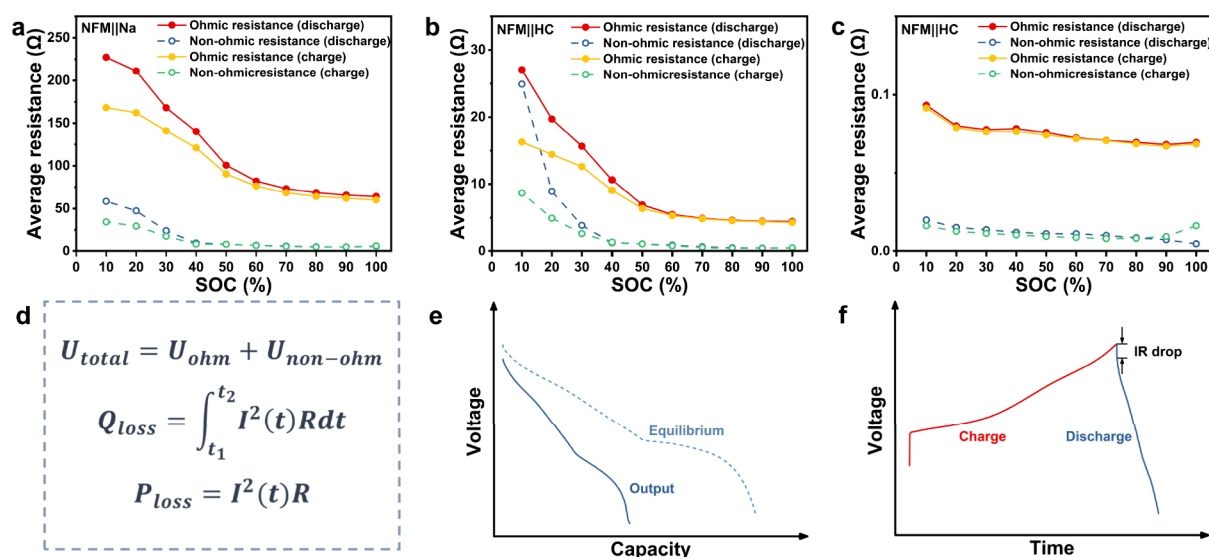


**Figure 4.** Impact of the cell assembly configuration on cell impedance. DCIR of (a) coin half cell, (b) coin full cell, and (c) pouch cell. (d) Formula for the influence of resistance on the overpotential ( $U$ ), energy ( $Q$ ), and power ( $P$ ) characteristics of the cell.<sup>22,23,26</sup> Schematic diagram of (e) output voltage deviating from the theoretical equilibrium potential and (f) potential drop between charge and discharge.

the cathode. The stacking process is repeated to obtain the multilayered pouch cell, and the reserved collectors of cathode or anode should coincide during the assembly process. Afterward, the stacked electrodes and separators are fixed with insulated tapes. The reserved collectors are subsequently trimmed to the same length and welded to aluminum tape. The height of adhesives across two tapes remains consistent to ensure good sealing after hot packing. Subsequently, the stacked electrodes are packed in the aluminum plastic film with three sealed sides and one open side for subsequent electrolyte filling. After addition of the electrolyte, the aluminum plastic pouch is hermetically sealed. The pouch cell should be clamped tightly in the fixture and undergo a resting period exceeding 12 h. After electrochemical activation with a small current, the gas generated during the formation process is evacuated, and the pouch is resealed for the subsequent electrochemical test (Figure S13). Notably, most air-sensitive layered cathode materials need to be assembled in a low-humidity environment (such as dry room or glovebox), thus preventing degradation of the pouch cells.

**Superiority and Application of Pouch Cell.** Nevertheless, there exist notable distinctions between coin cells and pouch cells, primarily concerning their cell impedance. The impedance of cells with different types is evaluated by the galvanostatic intermittent titration technique (GITT), direct current internal resistance (DCIR), and electrochemical impedance spectroscopy (EIS). The impedance in all cell types exhibits almost consistent trends that vary with voltage and SOC, where the impedance increases as the voltage and the SOC decreases during both the charging and discharging processes (Figures 4a–c, S14–S16). The EIS results reveal that  $\text{Na}^+$  ion migration resistance and charge-transfer resistance of the coin half cell (Figure S16) are significantly higher than those of the coin full cell, indicating the formation of unstable SEI due to the high reactivity of the metallic Na anode. Besides, GITT and DCIR results indicate a higher ohmic resistance in the coin cell ( $\sim 5.5 \Omega$  at 60% SOC) compared to the pouch cell ( $\sim 0.07 \Omega$  at 60% SOC) (Figures 4b,c, S14b,c, and S15), which is attributed to the disparities in cell configuration and internal component resistance. The total

overpotential ( $U_{\text{total}}$ ) can be summarized by the ohmic overpotential ( $U_{\text{ohm}}$ ) and nonohmic overpotential ( $U_{\text{nonohm}}$ ) (Figure 4d),<sup>30</sup> and the ohmic resistance constitutes a significant proportion of the cell's total resistance (Figure 4a–c) at the beginning of the cycle. Thus, the higher ohmic resistance in coin cells can lead to a notable increase in the cell's overpotential, which leads to increased energy spent ( $Q_{\text{loss}}$ ) and may induce detrimental phase transitions during charging process.<sup>31,32</sup> Additionally, during the discharging process, the rise in resistance and overpotential results in the output voltage deviating from the theoretical equilibrium potential (Figure 4e) and the internal resistance drop (IR drop) arises (Figure 4f), which consequently diminishes the efficiency, capacity and power ( $P_{\text{loss}}$ ) of cells, thus generating heat release and accelerating the deterioration of the battery performance.<sup>32–35</sup> Anyway, it can be consistently observed that the impedance of the half cells is higher than that of full cells, while the pouch cell exhibits significantly lower impedance than the coin cells. As a result, the cell types have a significant impact on the rate performance.

With the implementation of high mass-loading electrodes, the capacity of the half cell drops sharply at high rates, with the capacity at 4 C amounting to only 16% of that at 0.1 C (Figure S17a), indicating that the large impedance of the cell poses limitations on its rate capability and further revealing the voltage deviation and interfacial instability of the Na metal electrode at high current densities. In the full cell, the rate performance is improved significantly, and the impact on cell capacity arising from rate is further reduced in the pouch full cell (80% capacity maintained at 4 C, Figure S17b), demonstrating that the pouch cell configuration can maximize the release of capacity and enhance the fast charging ability. Except for the cell configuration and internal component resistance, variations in measured resistance fundamentally originate from electrolyte depletion and parasitic side reactions, whose severity differs across cell configurations. While cathode properties are inherently configuration-independent, different assembly methods and improper measurement may introduce experimental artifacts that obscure accurate cathode evaluation.

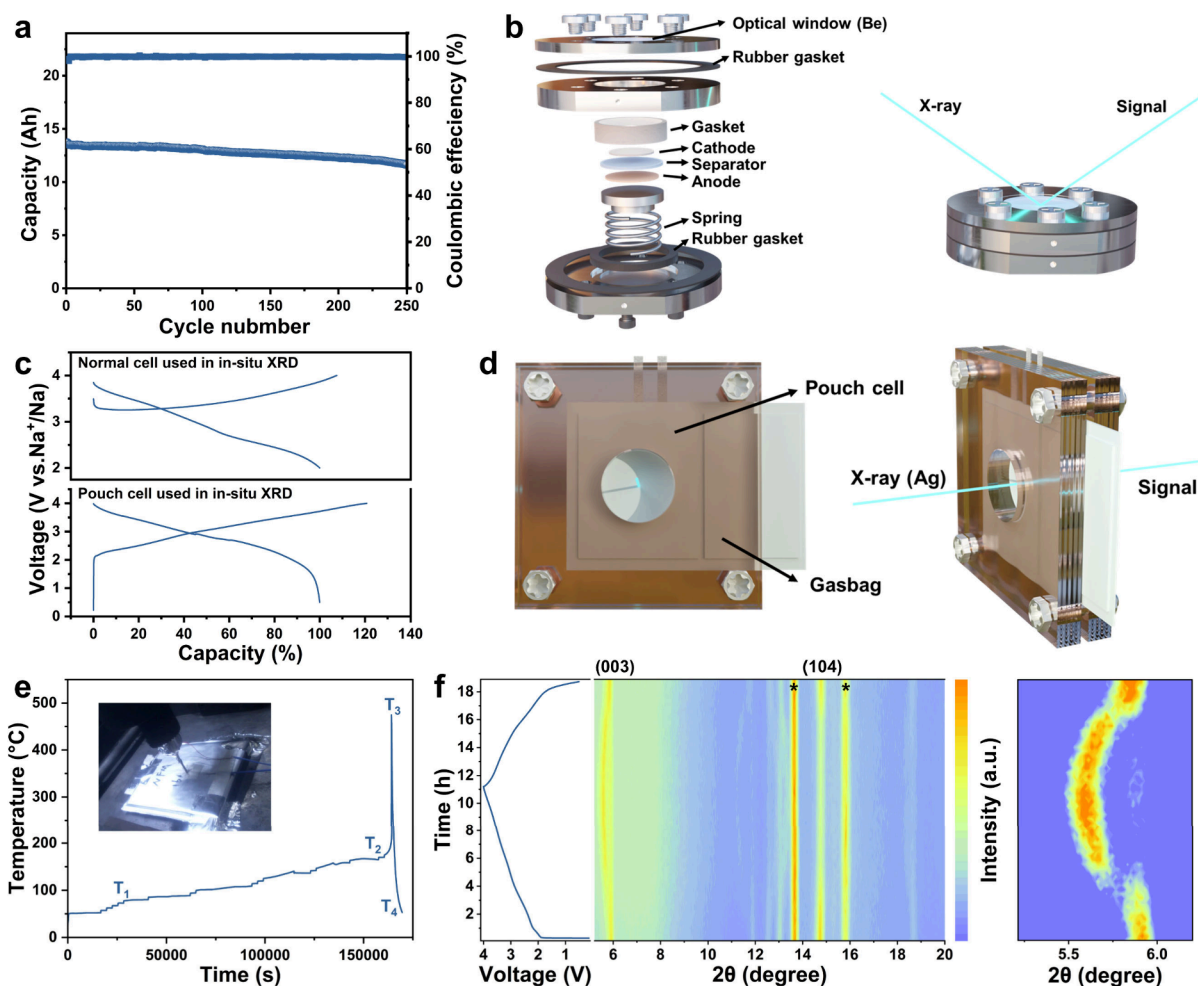


**Figure 5.** Advantages of pouch cells. (a) Cycling performance of the pouch cell. (b) Schematic diagram of the cell used for in situ XRD test. (c) First charging–discharging curves of cells used for in situ XRD. (d) Schematic diagram of pouch cell used for in situ XRD test. (e) Safety analysis of pouch cell at full charged state. (f) In-situ XRD result of pouch cell (“\*” represents the peak of Al).

The reliable pouch cell is advantageous for obtaining accurate electrochemical performance data and possesses a distinct edge in mechanism analysis compared with the coin cell. As presented in Figure 5a, the NFM||HC pouch cell delivers a capacity of 13 Ah with a high capacity retention of exceeding 85% for 250 cycles, surpassing most of the reported sodium ion batteries (Table S5).<sup>36–41</sup> Taking in situ X-ray diffraction (XRD) as an instance, the primary impact of cell configuration on in situ XRD analysis stems from current-induced polarization effects, which distort the actual potential of the working electrode, thereby complicating the precise correlation between structural evolution and electrode potential. Although the crystal structure evolution of the cathode material directly reflects the extent of sodium deintercalation, it is not absolutely synchronized with the measured cell voltage. In most academic research on SIBs and LIBs, a special cell employing beryllium (Be) metal as the optical window is employed to enhance X-ray transmission for in situ XRD test of active materials (Figure 5b). However, the high polarization of the coin analogue cell (the middle voltage is up to 3.39 V during charge) (Figure 5c) as well as the severe side reactions between Be and electrolyte result in a large deviation between the test system and the actual working conditions. In the in situ XRD tests with low-mass-loading ( $\sim 5 \text{ mg cm}^{-2}$ ) of NFM cathode using the coin-type electro-

chemical cell (simulating precise potential monitoring), different charging cutoff potentials will lead to different degrees of crystal evolution (Figure S18, compared with the NFM||Na cell charged to 4.0 V in our prior study<sup>42</sup>), highlighting the sensitivity of structural response to electrochemical conditions. In contrast, the pouch cell configuration in the in situ XRD test (Figure 5d) is close to operando characterization, which can trace the changes of active materials in the real state (Figure 5f). The in situ XRD results of the NFM||HC pouch cell show that the (003) peak shifts to a lower angle during charging, indicating the O3 phase of NFM transforms into the P3 phase with expansion of the structure *c*-axis. Benefiting from the measurement method, the powerful data about structure evolution of electrode can be further analyzed for a wide temperature range, high current, and so on. The measurement method can be utilized to observe the structural modifications of electrode materials in diverse environments, analyze the mutual interference between the positive and negative electrodes on the observation of the structural changes of electrode material, and obtain XRD signals of both positive and negative electrodes,<sup>43</sup> which promotes the development of electrochemical mechanisms. In addition, pouch cells can be utilized for battery safety analysis (Figures 5e, S19). Interestingly, the results of the accelerating rate calorimeter (ARC) exhibit a favorable safety of sodium ion

battery with layered NaTMO<sub>2</sub> as cathode, and the phenomenon of fire combustion is not observed after the nail penetration test, which is helpful to further evaluate the overall performance of sodium-ion batteries.

To conclude, HC-based pouch cells provide a reliable platform for accurately evaluating the electrochemical performance of cathodes, effectively overcoming the limitations of unstable sodium metal anodes (e.g., potential fluctuations, electrolyte decomposition, and electrode passivation). Systematic comparisons of electrochemical performance confirm that HC-based pouch cells exhibit better electrochemical performance than Na-based half cells, including lower Na<sup>+</sup> ion migration and charge-transfer resistance, superior cycling stability (95% cycling retention in 100 cycles vs ~70% of NFM//Na half cells), and enhanced rate performance (80% capacity retention at 4 C vs only ~20% of NFM//Na half cells), highlighting the interfacial and structural stability of HC anodes. Additionally, we outline critical parameters, including slurry preparation protocols, N/P ratio optimization, and cell assembly procedures, thus ensuring the reproducible fabrication of high-mass-loading HC-based full cells. Furthermore, the lower current-induced polarization stemming from the lower ohmic resistance of the pouch cell configuration enables precise mechanism analysis under real operating conditions, offering a robust methodology to evaluate lab-developed cathode materials and bridging the gap between academic research and industrial applications.

## ■ ASSOCIATED CONTENT

### Supporting Information

The Supporting Information is available free of charge at <https://pubs.acs.org/doi/10.1021/acsenergylett.5c00479>.

Experiment methods, characterizations, and additional electrochemical data (DOCX)

## ■ AUTHOR INFORMATION

### Corresponding Authors

**Yang Yang** – State Key Laboratory of Physical Chemistry of Solid Surfaces, State-Province Joint Engineering Laboratory of Power Source Technology for New Energy Vehicle, College of Chemistry and Chemical Engineering, Xiamen University, Xiamen 361005, P. R. China; [orcid.org/0000-0003-4215-5767](https://orcid.org/0000-0003-4215-5767); Email: [yangyang419@xmu.edu.cn](mailto:yangyang419@xmu.edu.cn)

**Jinbao Zhao** – State Key Laboratory of Physical Chemistry of Solid Surfaces, State-Province Joint Engineering Laboratory of Power Source Technology for New Energy Vehicle, College of Chemistry and Chemical Engineering, Xiamen University, Xiamen 361005, P. R. China; [orcid.org/0000-0002-2753-7508](https://orcid.org/0000-0002-2753-7508); Email: [jbzhao@xmu.edu.cn](mailto:jbzhao@xmu.edu.cn)

### Authors

**Huiya Yang** – State Key Laboratory of Physical Chemistry of Solid Surfaces, State-Province Joint Engineering Laboratory of Power Source Technology for New Energy Vehicle, College of Chemistry and Chemical Engineering, Xiamen University, Xiamen 361005, P. R. China

**Yuejing Zeng** – State Key Laboratory of Physical Chemistry of Solid Surfaces, State-Province Joint Engineering Laboratory of Power Source Technology for New Energy Vehicle, College of Chemistry and Chemical Engineering, Xiamen University, Xiamen 361005, P. R. China

**Wei Li** – State Key Laboratory of Physical Chemistry of Solid Surfaces, State-Province Joint Engineering Laboratory of Power Source Technology for New Energy Vehicle, College of Chemistry and Chemical Engineering, Xiamen University, Xiamen 361005, P. R. China

Complete contact information is available at:

<https://pubs.acs.org/doi/10.1021/acsenergylett.5c00479>

## Notes

The authors declare no competing financial interest.

## ■ ACKNOWLEDGMENTS

We gratefully acknowledge the financial support of National Key Research and Development Program of China (2021YFB2400300), National Natural Science Foundation of China (21875198, 21875195, 22109030, 22021001, 22379125), Natural Science Foundation of Fujian Province of China (2019A1515111069). We also acknowledge the help of Tan Kah Kee Innovation Laboratory on the scientific tests. The authors would particularly like to acknowledge my groupmates Minghao Zhang, Sirui Lin, and Kaiwen Li, for their wonderful collaboration and patient support.

## ■ REFERENCES

- (1) Goikolea, E.; Palomares, V.; Wang, S.; de Larramendi, I. R.; Guo, X.; Wang, G.; Rojo, T. Na-Ion Batteries—Approaching Old and New Challenges. *Adv. Energy Mater.* **2020**, *10* (44), 2002055.
- (2) Guo, Y.-J.; Jin, R.-X.; Fan, M.; Wang, W.-P.; Xin, S.; Wan, L.-J.; Guo, Y.-G. Sodium Layered Oxide Cathodes: Properties, Practicality and Prospects. *Chem. Soc. Rev.* **2024**, *53* (15), 7828–7874.
- (3) Usiskin, R.; Lu, Y. X.; Popovic, J.; Law, M.; Balaya, P.; Hu, Y.-S.; Maier, J. Fundamentals, Status and Promise of Sodium-Based Batteries. *Nat. Rev. Mater.* **2021**, *6* (11), 1020–1035.
- (4) Liang, X.; Hwang, J.; Sun, Y. Practical Cathodes for Sodium-ion Batteries: Who Will Take the Crown? *Adv. Energy Mater.* **2023**, *13* (37), 2301975.
- (5) Zhang, H.; Gao, Y.; Liu, X. H.; Zhou, L. F.; Li, J. Y.; Xiao, Y.; Peng, J.; Wang, J. Z.; Chou, S. Long-cycle-life Cathode Materials for Sodium-ion Batteries toward Large-scale Energy Storage Systems. *Adv. Energy Mater.* **2023**, *13* (23), 2300149.
- (6) Zuo, W.; Innocenti, A.; Zarrabeitia, M.; Bresser, D.; Yang, Y.; Passerini, S. Layered Oxide Cathodes for Sodium-Ion Batteries: Storage Mechanism, Electrochemistry, and Techno-Economics. *Acc. Chem. Res.* **2023**, *56* (3), 284–296.
- (7) Huang, S.; Sun, Y.; Yuan, T.; Che, H.; Zheng, Q.; Zhang, Y.; Li, P.; Qiu, J.; Pang, Y.; Yang, J.; Ma, Z.-F.; Zheng, S. Mitigating Voltage Decay of O<sub>3</sub>-NaNi<sub>1/3</sub>Fe<sub>1/3</sub>Mn<sub>1/3</sub>O<sub>2</sub> Layered Oxide Cathode for Sodium-Ion Batteries by Incorporation of 5d Metal Tantalum. *Carbon Neutralization* **2024**, *3* (4), 584–596.
- (8) Li, P.; Yuan, T.; Qiu, J.; Che, H.; Ma, Q.; Pang, Y.; Ma, Z.-F.; Zheng, S. A Comprehensive Review of Layered Transition Metal Oxide Cathodes for Sodium-Ion Batteries: The Latest Advancements and Future Perspectives. *Mater. Sci. Eng.: R: Rep.* **2025**, *163*, 100902.
- (9) Yuan, T.; Li, P.; Sun, Y.; Che, H.; Zheng, Q.; Zhang, Y.; Huang, S.; Qiu, J.; Pang, Y.; Yang, J.; Ma, Z.-F.; Zheng, S. Refining O<sub>3</sub>-Type Ni/Mn-Based Sodium-Ion Battery Cathodes via “Atomic Knife” Achieving High Capacity and Stability. *Adv. Funct. Mater.* **2025**, *35* (5), 2414627.
- (10) Hu, J.; Wu, B.; Chae, S.; Lochala, J.; Bi, Y.; Xiao, J. Achieving Highly Reproducible Results in Graphite-Based Li-Ion Full Coin Cells. *Joule* **2021**, *5* (5), 1011–1015.
- (11) Chen, S.; Niu, C.; Lee, H.; Li, Q.; Yu, L.; Xu, W.; Zhang, J.-G.; Dufek, E. J.; Whittingham, M. S.; Meng, S.; Xiao, J.; Liu, J. Critical Parameters for Evaluating Coin Cells and Pouch Cells of Rechargeable Li-Metal Batteries. *Joule* **2019**, *3* (4), 1094–1105.

- (12) Li, H. Practical Evaluation of Li-Ion Batteries. *Joule* **2019**, *3* (4), 911–914.
- (13) Zheng, X.; Huang, L.; Ye, X.; Zhang, J.; Min, F.; Luo, W.; Huang, Y. Critical Effects of Electrolyte Recipes for Li and Na Metal Batteries. *Chem.* **2021**, *7* (9), 2312–2346.
- (14) Murray, V.; Hall, D. S.; Dahn, J. R. A Guide to Full Coin Cell Making for Academic Researchers. *J. Electrochem. Soc.* **2019**, *166* (2), A329.
- (15) Sun, Y.; Li, J.-C.; Zhou, H.; Guo, S. Wide-Temperature-Range Sodium-Metal Batteries: From Fundamentals and Obstacles to Optimization. *Energy Environ. Sci.* **2023**, *16* (11), 4759–4811.
- (16) Stevens, D. A.; Dahn, J. R. High Capacity Anode Materials for Rechargeable Sodium-Ion Batteries. *J. Electrochem. Soc.* **2000**, *147* (4), 1271.
- (17) Chu, Y.; Zhang, J.; Zhang, Y.; Li, Q.; Jia, Y.; Dong, X.; Xiao, J.; Tao, Y.; Yang, Q.-H. Reconfiguring Hard Carbons with Emerging Sodium-Ion Batteries: A Perspective. *Adv. Mater.* **2023**, *35* (31), 2212186.
- (18) Zeng, Y.; Yang, J.; Yang, H.; Yang, Y.; Zhao, J. Bridging Microstructure and Sodium-Ion Storage Mechanism in Hard Carbon for Sodium Ion Batteries. *ACS Energy Lett.* **2024**, *9* (3), 1184–1191.
- (19) Wang, Y.; Li, M.; Zhang, Y.; Zhang, N. Hard Carbon for Sodium Storage: Mechanism and Performance Optimization. *Nano Res.* **2024**, *17* (7), 6038–6057.
- (20) Wang, X.; Lu, J.; Wu, Y.; Zheng, W.; Zhang, H.; Bai, T.; Liu, H.; Li, D.; Ci, L. Building Stable Anodes for High-Rate Na-Metal Batteries. *Adv. Mater.* **2024**, *36* (16), 2311256.
- (21) An, Z.; Shi, T.; Zhao, Y.; Gong, Q.; Zhang, D.; Bai, J.; Du, X. Study on Aging and External Short Circuit Mechanisms of Li-Ion Cells with Different Electrode Thicknesses. *Appl. Energy* **2023**, *350*, 121796.
- (22) Faraji Niri, M.; Reynolds, C.; Román Ramírez, L. A.; Kendrick, E.; Marco, J. Systematic Analysis of the Impact of Slurry Coating on Manufacture of Li-Ion Battery Electrodes via Explainable Machine Learning. *Energy Storage Mater.* **2022**, *51*, 223–238.
- (23) Zhang, Y.; Bailey, J.; Sun, Y.; Boyce, A. M.; Dawson, W.; Reynolds, C. D.; Zhang, Z.; Lu, X.; Grant, P.; Kendrick, E.; Shearing, P.; Brett, D. Applications of Advanced Metrology for Understanding the Effects of Drying Temperature in Lithium-Ion Battery Electrodes Manufacturing Process. *J. Mater. Chem. A* **2022**, *10*, 10593–10603.
- (24) Cao, Y.; Li, M.; Lu, J.; Liu, J.; Amine, K. Bridging the Academic and Industrial Metrics for Next-Generation Practical Batteries. *Nat. Nanotechnol.* **2019**, *14* (3), 200–207.
- (25) Wang, Y.; Liu, B.; Tian, G.; Qi, S.; Wu, D. Research Progress of Cathode Binder for High Performance Lithium-Ion Battery. *Acta Polym. Sin.* **2020**, *51* (4), 326–337.
- (26) Ma, F.; Fu, Y.; Battaglia, V.; Prasher, R. Microrheological Modeling of Lithium Ion Battery Anode Slurry. *J. Power Sources* **2019**, *438*, 226994.
- (27) Yang, Y.; Wu, C.; He, X.-X.; Zhao, J.; Yang, Z.; Li, L.; Wu, X.; Li, L.; Chou, S.-L. Boosting the Development of Hard Carbon for Sodium-Ion Batteries: Strategies to Optimize the Initial Coulombic Efficiency. *Adv. Funct. Mater.* **2024**, *34* (5), 2302277.
- (28) Chen, Z.; Zhang, L.; Wu, X.; Song, K.; Ren, B.; Li, T.; Zhang, S. Effect of N/P Ratios on the Performance of  $\text{LiNi}_{0.8}\text{Co}_{0.15}\text{Al}_{0.05}\text{O}_2$ || $\text{SiO}_x$ /Graphite Lithium-Ion Batteries. *J. Power Sources* **2019**, *439*, 227056.
- (29) Zhang, Y.; Wang, H.; Li, Z.; Ge, X.; Huang, K.; Huang, J.-Q.; Huang, L.; Li, Z.; Huang, Y. Innovative Anode Design to Enhance Both Volumetric and Gravimetric Energy Densities of  $\text{LiCoO}_2$ ||graphite Pouch Cells. *Adv. Energy Mater.* **2025**, *15* (10), 2403804.
- (30) Zhang, L.; Wang, L.; Lyu, C.; Li, J.; Zheng, J. Non-Destructive Analysis of Degradation Mechanisms in Cycle-Aged Graphite/LiCoO<sub>2</sub> Batteries. *Energies* **2014**, *7* (10), 6282–6305.
- (31) Yue, Y.; Li, S.; Cheng, X.; Wei, J.; Zeng, F.; Zhou, X.; Yang, J. Effects of Temperature on the Ohmic Internal Resistance and Energy Loss of Lithium-Ion Batteries under Millisecond Pulse Discharge. *J. Phys. Conf. Ser.* **2022**, *2301* (1), No. 012014.
- (32) Liu, C.; Neale, Z. G.; Cao, G. Understanding Electrochemical Potentials of Cathode Materials in Rechargeable Batteries. *Mater. Today* **2016**, *19* (2), 109–123.
- (33) Son, Y.; Cha, H.; Lee, T.; Kim, Y.; Boies, A.; Cho, J.; De Volder, M. Analysis of Differences in Electrochemical Performance between Coin and Pouch Cells for Lithium-Ion Battery Applications. *Energy Environ. Mater.* **2024**, *7* (3), No. e12615.
- (34) Zhao, C.; Yin, H.; Yang, Z.; Ma, C. Equivalent Series Resistance-Based Energy Loss Analysis of a Battery Semiactive Hybrid Energy Storage System. *IEEE Trans. Energy Convers.* **2015**, *30* (3), 1081–1091.
- (35) Xiong, R.; Yu, Y.; Chen, S.; et al. Overpotential Decomposition Enabled Decoupling of Complex Kinetic Processes in Battery Electrodes. *J. Power Sources* **2023**, *553*, 232296.
- (36) Altin, E.; Moez, I.; Kwon, E.; Bhatti, A. H. U.; Yu, S.; Chung, K. Y.; Arshad, M.; Harfouche, M.; Buldu, M.; Altundag, S.; Bulut, F.; Sahinbay, S.; Altin, S.; Ates, M. N. Revealing the Role of Ruthenium on the Performance of P2-Type  $\text{Na}_{0.67}\text{Mn}_{1-x}\text{Ru}_x\text{O}_2$  Cathodes for Na-Ion Full-Cells. *Small* **2024**, *20* (50), 2406332.
- (37) Dogan, E.; Whba, R.; Altin, E.; Moez, I.; Chung, K. Y.; Stoyanova, R.; Koleva, V.; Aktas, A.; Altin, S.; Sahinbay, S. Optimized Performance of  $\text{Na}_{0.67}\text{Mn}_{0.5}\text{Fe}_{0.5}\text{O}_2$ @ $\text{TiO}_2$  and Presodiated Hard Carbon (Pre-SHC) Full-Cells Using Direct Contact Method. *J. Power Sources* **2025**, *632*, 236327.
- (38) Kalyoncuoglu, B.; Ozgul, M.; Altundag, S.; Bulut, F.; Oz, E.; Sahinbay, S.; Altin, S. High-Performance Na-Ion Full-Cells with P2-Type  $\text{Na}_{0.67}\text{Mn}_{0.5-x}\text{Ni}_x\text{Fe}_{0.43}\text{Al}_{0.07}\text{O}_2$  Cathodes: Cost Analysis for Stationary Battery Storage Systems. *J. Energy Storage* **2024**, *79*, 110203.
- (39) Zhang, K.; Xu, Z.; Li, G.; Luo, R.; Ma, C.; Wang, Y.; Zhou, Y.; Xia, Y. Regulating Phase Transition and Oxygen Redox to Achieve Stable High-voltage O3-type Cathode Materials for Sodium-ion Batteries. *Adv. Energy Mater.* **2023**, *13*, 2302793.
- (40) Ding, F.; Ji, P.; Han, Z.; Hou, X.; Yang, Y.; Hu, Z.; Niu, Y.; Liu, Y.; Zhang, J.; Rong, X.; Lu, Y.; Mao, H.; Su, D.; Chen, L.; Hu, Y.-S. Tailoring Planar Strain for Robust Structural Stability in High-Entropy Layered Sodium Oxide Cathode Materials. *Nat. Energy* **2024**, *9* (12), 1529–1539.
- (41) Zhang, S.; Li, X.; Su, Y.; Yang, Y.; Yu, H.; Wang, H.; Zhang, Q.; Lu, Y.; Song, D.; Wang, S.; Zhang, Q.; Rong, X.; Zhang, L.; Chen, L.; Hu, Y.-S. Four-In-One Strategy to Boost the Performance of  $\text{Na}_x[\text{Ni},\text{Mn}]\text{O}_2$ . *Adv. Funct. Mater.* **2023**, *33* (36), 2301568.
- (42) Yang, H.; Zhang, Q.; Chen, M.; Yang, Y.; Zhao, J. Unveiling the Origin of Air Stability in Polyanion and Layered-oxide Cathode Materials for Sodium-ion Batteries and Their Practical Application Considerations. *Adv. Funct. Materials* **2024**, *34*, 2308257.
- (43) Wu, Q.; Kang, Y.; Chen, G.; Chen, J.; Chen, M.; Li, W.; Lv, Z.; Yang, H.; Lin, P.; Qiao, Y.; Zhao, J.; Yang, Y. Ultrafast Carbothermal Shock Synthesis of Wadsley–Roth Phase Niobium-Based Oxides for Fast-Charging Lithium-Ion Batteries. *Adv. Funct. Mater.* **2024**, *34* (23), 2315248.